



Novel and adaptive contribution of the red channel in pre-processing of colour fundus images

Nancy M. Salem, Asoke K. Nandi*

*Signal Processing and Communications Group, Department of Electrical Engineering and Electronics,
The University of Liverpool, Brownlow Hill, L69 3GJ, Liverpool, UK*

Received 22 December 2005; received in revised form 12 September 2006; accepted 12 September 2006

Abstract

A new pre-processing method for colour fundus images with adaptive contribution of the red channel is proposed. Based on a condition that is developed in this paper, this method utilises the intensity information from both red and green channels instead of using only the green channel as in the usual practice. The histogram matching is used to modify the histogram of the green channel by using the histogram of the red channel (of the same retinal image) to obtain a new processed image having the advantages of both channels. This method can be used to correct non-uniform illumination in colour fundus images or as a pre-processing step in the automatic analysis of retinal images.

Results show that the use of histogram matched (HM) image give better performance than using the green channel image when employing the two-dimensional matched filter to detect retinal blood vessels. At specificity of 90%, in case of abnormal images, sensitivity increased from 76% when using the green channel image to 82% when using the HM image compared with 81% when using the piece-wise threshold probing method. In case of normal images, at the same specificity, the sensitivity obtained when using green channel image or HM image was 87% compared with 88% for the piece-wise threshold probing method.

© 2006 The Franklin Institute. Published by Elsevier Ltd. All rights reserved.

Keywords: Medical image processing; Retinal images; Histogram matching

*Corresponding author. Tel.: +44 151 7944525; fax: +44 151 7944540.

E-mail addresses: nancy.salem@liverpool.ac.uk (N.M. Salem), A.Nandi@liverpool.ac.uk (A.K. Nandi).

1. Introduction

Automatic analysis of retinal images is a challenging research area that aims to provide automated methods to help in the early detection and diagnosis of many eye diseases such as diabetic retinopathy and age-related macular degeneration (AMD). Retinal images pre-processing, segmentation, and analysis are different forms of contributions for digital image processing techniques in this area.

Diabetic retinopathy remains the commonest cause of new blindness in the working age population in the UK [1]. Up to 98% of visual loss from diabetic retinopathy can be prevented by timely treatment [2,3]. Image processing techniques can contribute to the early detection and diagnosis of diabetic retinopathy in image enhancement, mass screening, and monitoring of the disease [4]. Diabetic retinopathy meets all the criteria for a disease that warrant screening, it has a long latent period before visual loss and is eminently treatable. As well, screening for retinopathy is non-invasive, cost-effective, and highly sensitive and specific [5].

AMD is now the leading cause of blindness in the developed countries [3] and the most common cause of vision loss in people over 50 years of age [6]. Over the last two decades, there has been continued interest in the use of digital techniques for quantification of macular pathology, particularly drusen [7]. Drusen identification and measurement play a key role in clinical studies of this disease. Current manual methods of drusen measurements are laborious and subjective, and there is a potential for use automated techniques [7,8] for detection and quantification of drusen in retinal images which will help in early detection and treatment of AMD.

Pre-processing of retinal images in the literature is used to reduce the effect of noise [9], help in the detection of anatomical structures [10,11], colour normalisation of retinal images [12,13], visual image quality assessment [14], and automatic mask generation [15]. Retinal images were smoothed by a 5×5 mean filter to reduce the effect of spurious noise in [9] and transformed using wavelet transform in [10], where the optic nerve head was enhanced by modifying the wavelet coefficients by suppressing the small scale coefficients and enhancing the larger scale coefficients. To detect the main components of the fundus, i.e. the optic disc, fovea, and blood vessels, Sinthanayothin et al. [11] presented a pre-processing step to reduce the effect of changing the contrast in different regions of the fundus image and to normalise the mean intensity. This was accomplished by transforming the intensities of the three colour bands to an intensity-hue-saturation representation, then enhancing the contrast of the intensity by a locally adaptive transformation.

Histogram matching was proven to be a good normalisation method for making colour images invariant with respect to background pigmentation variation between individuals, by selecting a particular retinal image as a reference image and use the histogram matching to modify the three channels of each colour image, which solve the problem of wide variations in the colour of the fundus from different patients [12] and improve the clustering of the different lesion types [13]. Histogram matching is also used in visual image quality assessment [14], where model histograms for the pixel and edge value distributions are used, these models were defined using a set of good quality images.

The region of interest in retinal images is the field of view (FOV) which contains anatomical structures as well as lesions abnormalities of anatomical structures. Mask generation aims to avoid processing the black region that surrounds the FOV of retinal images which will result in decreasing the required processing time. In [15], statistical

measures are calculated for each colour channel of the image followed by a 4-sigma thresholding with a free parameter empirically chosen such that pixels with intensity value above that threshold are considered to belong to the FOV. Then, results for all bands are combined through logical operations and region connectivity test in order to identify the largest common mask.

Automatic segmentation of blood vessels in retinal images is an important step in screening programs for early detection of diabetic retinopathy [16], registration of retinal images for treatment evaluation [17] (to follow the evaluation of some lesions over the years or to compare images obtained under different conditions), generating retinal map for the diagnosis and treatment of AMD [18], or locating the optic disc and the fovea [19,20].

In this study, we propose a novel contribution of the red channel gray-level distributions with a novel application of the histogram matching approach other than colour normalisation. Here we utilise the intensity information from red and green channels of the same retinal image without using a reference image, as it is believed that each image has its own gray-level distributions according to the FOV, location of optic disc, normality, or abnormality. We are interested in using the red channel in pre-processing of colour fundus images for two reasons: firstly, to improve the visual appearance of retinal images in cases of non-uniform illumination and secondly, to improve the performance of blood vessels segmentation methods, which will be a helpful step towards the automatic analysis of retinal images.

As many methods are based on applying the two-dimensional matched filter [9] before segmenting retinal blood vessels [21–24], it is used here as an example and the effect of using red channel, green channel, and HM image on the efficiency of blood vessels detection is investigated. Performances of automatic detection of retinal blood vessels using HM images that result from the proposed method and using different reference histograms are investigated and results are compared with the piece-wise threshold probing method [21].

This paper is organised as follows, the proposed pre-processing method is outlined in Section 2. Experiments carried out to evaluate the performance of the proposed method are detailed in Section 3. Results and discussion are presented in Section 4 and the paper is summarised in Section 5.

2. Method

Unsupervised methods for segmenting blood vessels in colour fundus images use the green channel [9,21,23–25] because generally it has the highest contrast between blood vessels and the retinal background while the red channel is rather saturated and the blue channel is rather dark. Gray-level distributions of three (red, green, and blue) channels for a colour fundus image are shown in Fig. 1. For the same reason, green channel is used in supervised methods to detect image ridges [26] or to extract features [27] for pixels that will be classified as vessels or not. Experiments show that the red channel has the advantages of being brighter and distributed over a wider range of gray-level values, than the green channel, which results in less contrast between abnormalities and the retinal background.

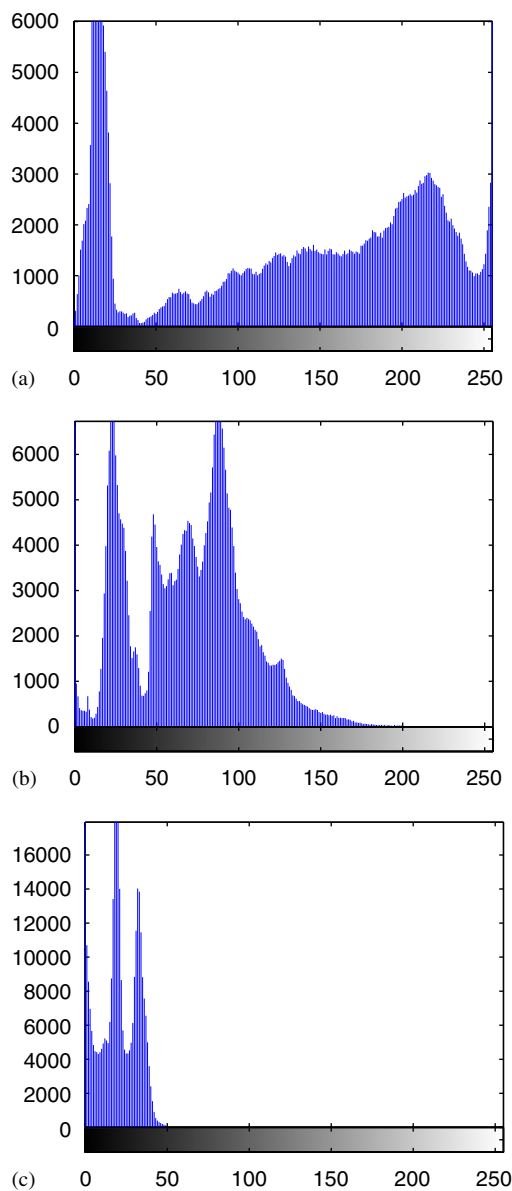


Fig. 1. Gray-level distributions in (a) red channel; (b) green channel; and (c) blue channel of one fundus image.

2.1. Histogram matching

Histogram matching is an approach that is used to generate a processed image that has a specified histogram [28], it has the advantage of producing more realistic looking images than those generating by equalisation. In the proposed method, we use the concept of histogram matching to modify the histogram of the green channel image to match that of

the red channel image in order to combine the distributions of gray-levels of both images. The procedures are summarised as follows:

- (1) Obtain histograms of both images (green and red channels).
- (2) Perform a mapping from the levels in the green channel image g_k into corresponding levels s_k based on its histogram.

$$\begin{aligned} s_k &= T(g_k) = \sum_{j=0}^k P_g(g_j) \\ &= \sum_{j=0}^k \frac{n_j}{n}, \quad k = 0, 1, 2, \dots, (L-1), \end{aligned} \quad (1)$$

where $P_g(g)$ is the probability density function for the green channel image, n is the total number of pixels in the image, n_j is the number of pixels with gray-level g_j , and L is the number of discrete gray-levels.

- (3) From $P_r(r)$, the histogram of the red channel image, obtain a transformation function G such that

$$G(r_k) = \sum_{j=0}^k P_r(r_j) = s_k, \quad k = 0, 1, 2, \dots, (L-1). \quad (2)$$

- (4) By using the inverse transform, we obtain:

$$r_k = G^{-1}[T(g_k)], \quad k = 0, 1, 2, \dots, (L-1) \quad (3)$$

or

$$r_k = G^{-1}(s_k), \quad k = 0, 1, 2, \dots, (L-1). \quad (4)$$

Theoretically, we are seeking values of r that satisfy Eq. (4).

- (5) Practically, for each gray-level g_k , map this value to its corresponding level s_k ; then map level s_k into the final level r_k .

2.2. Saturation condition

By comparing results of applying our proposed method to a set of test images, it is clear that the histogram of the red channel image affect the performance of the proposed method. For very bright images, using the histogram of the red channel to modify that of the green channel results in decreasing the contrast between retinal blood vessels and their background, which leads to a HM image with contrast much lower than the contrast in the green channel image. In these cases (of saturated images), the use of green channel images is preferred over the use of HM images. For this reason, a criterion to test the saturation of the red channel image is necessary to establish whether the green channel image or the HM image will be used.

In our experiments it has been observed that the histogram of very bright images is characterised by a large gap in the gray-level distributions, (see Fig. 2). This large gap in

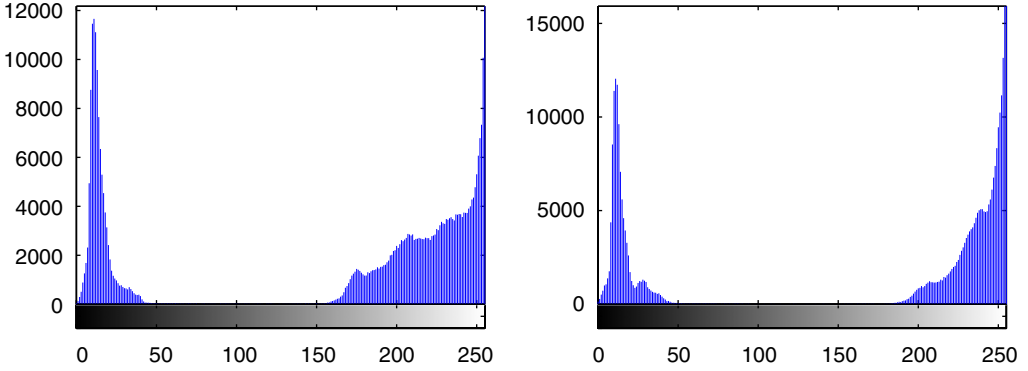


Fig. 2. Red channel histograms of two very bright (saturated) fundus images.

the observed histograms is caused by the pixels around the FOV having a very low values and the over-saturated pixels within the FOV having a very high values. There are many ways to detect this characteristic. Having experimented with different criteria, a computationally simple yet an effective criterion is as follows: calculate the cumulative summation of the gray-levels probability density function in the red channel up to the mean value:

$$\mu_r = \sum_{j=0}^{L-1} r_j \cdot P_r(r_j), \quad (5)$$

$$C_k = \sum_{j=0}^k P_r(r_j), \quad (6)$$

where $P_r(r)$ is the probability density function for the red channel image, k is the bin containing the mean value, μ_r , and L is the number of discrete gray-levels. The condition we use to test the saturation of a test image is

$$C_{\mu_r} \geq 0.3.$$

This value has been determined experimentally (see Section 4.2).

3. Experiments

In our experiments, we start by enhancing the visual appearance of a retinal image as a whole by processing the histogram of the green channel in conjunction with the histogram of the red channel as described earlier. Then, to test the effect of this enhancement on the appearance of blood vessels, we implement the algorithm in [9] to test the ability of the two-dimensional matched filter to segment blood vessels in retinal images. The red channel, green channel, and the HM images are used to obtain the matched filter response (MFR) images for every test image in the dataset.

For the purposes of comparison, we select three normal images from the dataset (that seemed to show the least non-uniform illumination) as reference images [12], the green channel histograms of these images are used as reference model histograms. The histogram

matching is used to modify the green channel of test images using these reference histograms in a similar way as in Eqs. (1)–(4).

To evaluate the performance of our proposed method, we use a dataset of 20 images publicly available [29]. These images are digitised slides captured by a TopCon TRV-50 fundus camera at 35° FOV. Each slide was digitised to produce a 605×700 pixels image, standard RGB, 8 bits per colour channel. Every image has been manually segmented by two observers to produce ground truth vessels segmentation. Ten of these images contain pathology and the other ten are normal, giving a good opportunity to test the proposed method in both normal and abnormal retinas. On average, the first observer labelled 32 200 pixels in each image as vessel, while the second observer labelled 46 100 pixels in each image as vessel. Subsequent review indicated that the first person took a more conservative view of the boundaries of vessels and in the identification of small vessels than the second observer [21]. The manual segmentation by the first observer is chosen as the ground truth for vessel segmentation.

The performance is also measured with receiver operating characteristic (ROC) curves [30,31]. An ROC curve plots the false positive rates against the true positive rates, and these rates are defined in the same way as in [21], where the true (false) positive is any pixel which was hand-labelled as a vessel (not vessel), whose MFR is above a given threshold. The true (false) positive rate is established by the dividing the number of true (false) positives by the total number of pixels hand-labelled as vessels (not vessels). The larger is the area under the ROC curve, the better is the performance of the algorithm.

4. Results and discussion

4.1. Results

The first application of our proposed method is to correct the non-uniform illumination, which is a common problem, in retinal images. Fig. 3 shows results of matching the green channel histogram with the red channel histogram for two test images. The HM image is

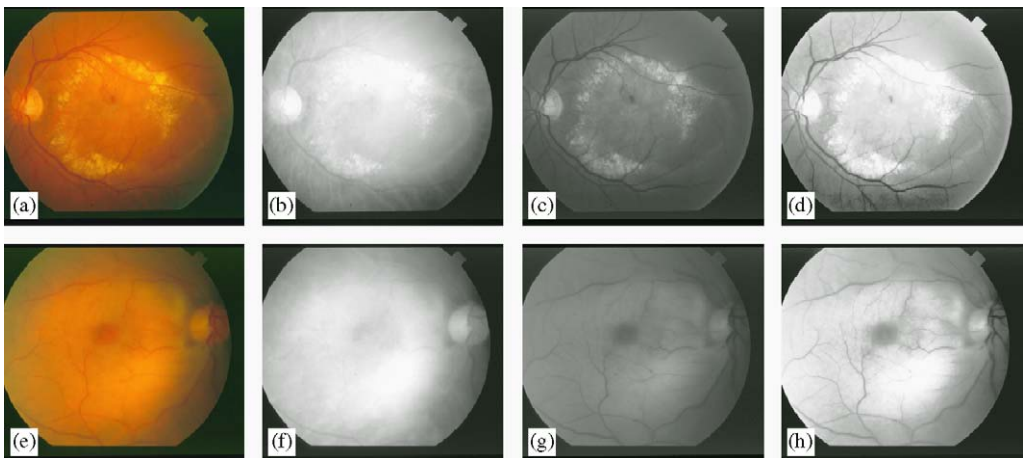


Fig. 3. Application of the proposed method for non-uniform illumination: (a,e) RGB images; (b,f) red channels; (c,g) green channels; and (d,h) HM images.

now a combination of the green channel image (which is less bright but with high contrast) and the red channel image (which is more uniformly illuminated).

The second application is to improve the performance of blood vessels detection methods. Retinal blood vessels are segmented using the method in [9], where the red channel, green channel, the HM images are used. Two types of HM images are used; the result of combining red and green histograms as well as the result of combining the green channel with three different reference histograms as shown in Fig. 4, ROC curves for these images plotted in Fig. 5. Average ROC curves for all 20 (normal and abnormal) images were considered for sensitivity and specificity analysis at some specified points and results are summarised in Table 1.

It is clear from Table 1 that for specificity of 90% or more, the red channel has the least sensitivity while the reference 3 offers the next least sensitivity followed by the green channel. The reference 1 and reference 2 are similar to each other and offer better sensitivity. The best sensitivity is achieved by the proposed HM image where the histogram of the red channel is used to modify that of the green channel.

As described earlier, we define a condition to test the saturation of the test image, so we will combine the information from the red and green channels as long as $C_{\mu} \geq 0.3$, otherwise we will use the green channel image in the segmentation of blood vessels. Figs. 6 and 7 show the average ROC curves for all images in the dataset after applying this condition.

Table 2 compares results using the green channel image, the proposed HM image when combining red and green channels, when using reference 1 histogram (best of the three reference histograms), and the results of applying the Hoover method [21].

4.2. Discussion

For efficient segmentation of retinal blood vessels, it is desirable to have high contrast between retinal blood vessels and the retinal background whilst there should be low

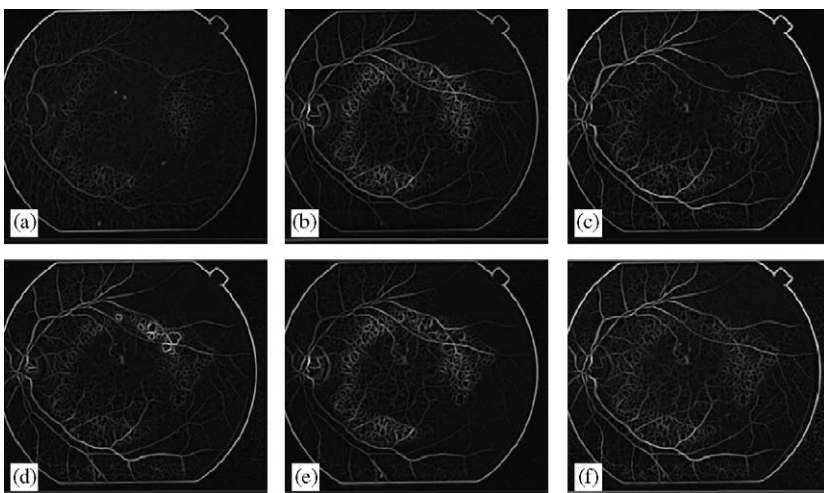


Fig. 4. Matched filter response images using (a) red channel; (b) green channel; and HM images when (c) combining red and green; (d,e,f) using three different reference models.

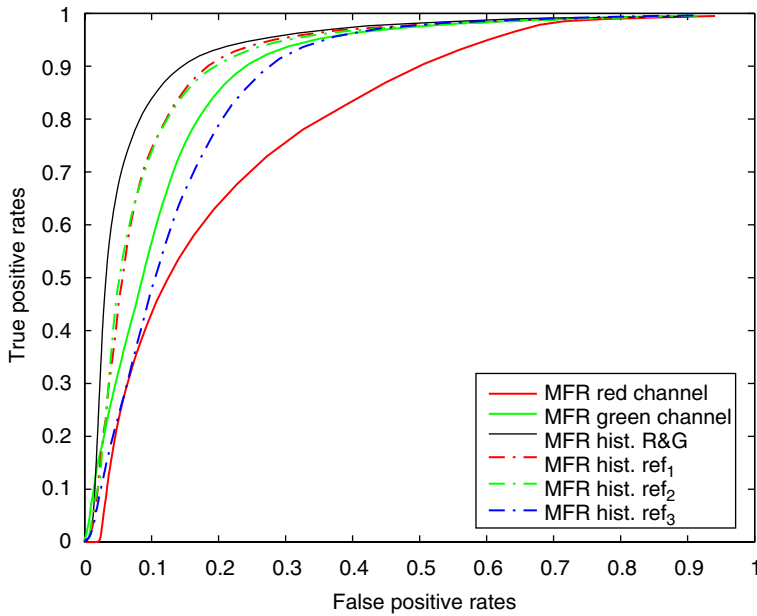


Fig. 5. ROC curves for images in Fig. 4.

Table 1

Sensitivity and specificity values before applying the saturation condition

| Specificity (%) | Image type | Sensitivity | | | | | |
|-----------------|------------|-------------|-----------|-----------|--------------------------|--------------------------|--------------------------|
| | | Red (%) | Green (%) | R & G (%) | G & Ref ₁ (%) | G & Ref ₂ (%) | G & Ref ₃ (%) |
| 95 | Normal | 53.16 | 71.38 | 73.45 | 72.42 | 72.58 | 58.82 |
| | Abnormal | 28.56 | 50.45 | 60.83 | 57.24 | 58.19 | 36.17 |
| | All images | 40.86 | 60.92 | 67.14 | 64.83 | 65.38 | 47.50 |
| 90 | Normal | 69.54 | 87.05 | 86.66 | 87.09 | 86.91 | 77.39 |
| | Abnormal | 48.15 | 76.46 | 79.83 | 78.40 | 78.15 | 59.85 |
| | All images | 58.85 | 81.75 | 83.41 | 82.74 | 82.53 | 68.62 |
| 85 | Normal | 75.64 | 91.08 | 90.67 | 91.37 | 91.11 | 85.49 |
| | Abnormal | 58.21 | 85.44 | 86.08 | 86.00 | 85.29 | 74.00 |
| | All images | 66.92 | 88.26 | 88.37 | 88.69 | 88.20 | 79.74 |
| 80 | Normal | 72.56 | 93.02 | 92.54 | 93.36 | 93.09 | 89.98 |
| | Abnormal | 65.16 | 89.67 | 89.37 | 89.94 | 89.13 | 82.29 |
| | All images | 72.37 | 91.35 | 90.96 | 91.65 | 91.11 | 86.14 |

contrast between the retinal background and retinal abnormalities. Combining advantages of both channels, brightness in red channel and high contrast in green channel, results in decreasing the contrast between abnormalities and the retinal background. This helps to reduce some responses, which do not resemble to any blood vessels and that would otherwise decrease the performance of blood vessels segmentation methods. This pre-

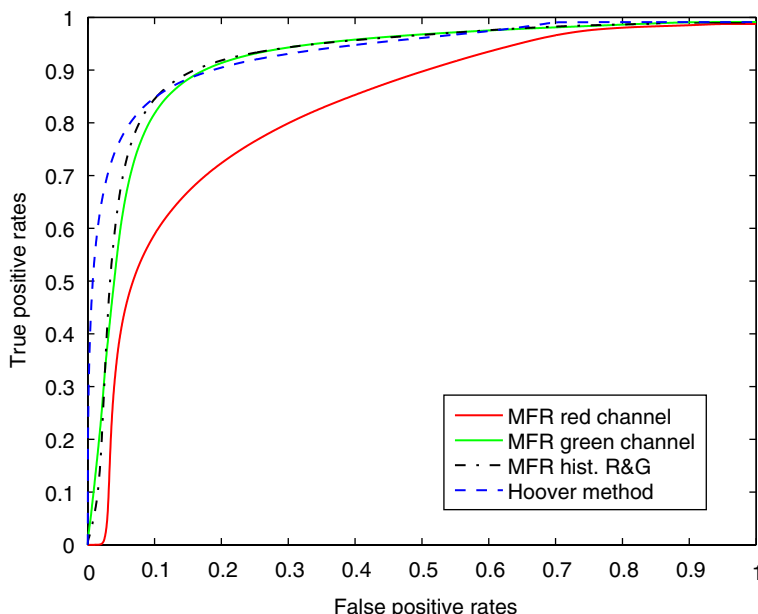


Fig. 6. Average ROC curves (after testing image saturation) for all images.

processing step takes about 1.04s to process an image on a Xeon 2.8 GHZ with 512 MB RAM using a MATLAB code (MATLAB V.7).

Figs. 3–5 show that the proposed combination of gray-level distributions from red and green channels is a useful pre-processing step in cases of non-uniform illumination and in improving the performance of blood vessels segmentation.

Histogram matching using reference histogram was useful in cases of normal images and very bright abnormal images; also results are affected by different choices of reference histograms (as seen in Table 1) which required an expert to select a suitable reference histogram. On the other hand, histogram matching using red and green histograms of the same image was useful in most of abnormal images, and to overcome the problem caused by very bright images (normal or abnormal), we use the saturation condition which improve the performance (as in Table 2). The reason behind setting a saturation condition is to establish whether to apply histogram matching or not. The value for C ($C < 0.3$) seems to define the set of very bright or saturated images that characterised with large gap in their histograms. Out of the 20 images, five images were excluded from the histogram matching and their green channel image are used for blood vessel segmentation. Further investigations will be carried on using a larger dataset in the future. Table 3 compares between average sensitivity before and after applying the saturation condition at specificity of 90%. Results before using the saturation condition are better than using the green channel only and further improved when using this condition, this is particularly noticeable for abnormal images.

To evaluate the performance of the proposed method, we compare between using MFR images generated using the HM image with results of Hoover et al. [21] (a segmentation method that require more post-processing), in which the MFR image (using the green channel) was probed. During each probing, the threshold of the probed region was

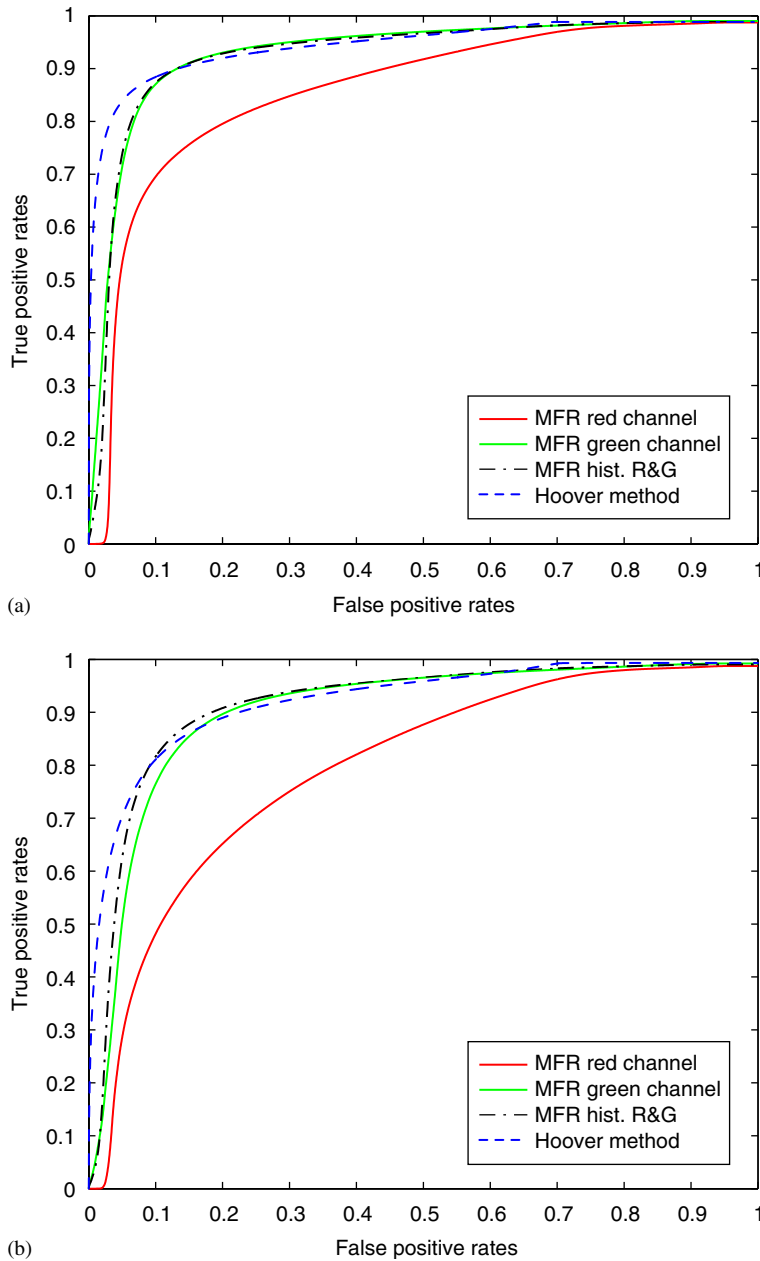


Fig. 7. Average ROC curves (after testing image saturation) for (a) normal images; (b) abnormal images.

determined according to testing a set of criteria, and ultimately it was decided if the area being probed was a blood vessel or not. MFR images generated using the HM images instead of the green channel image offer approximately the same performance as the Hoover method but without post-processing.

Table 2

Sensitivity and specificity values after applying the saturation condition

| Specificity (%) | Image type | Sensitivity | | | |
|-----------------|------------|-------------|-----------|--------------------------|------------|
| | | Green (%) | R & G (%) | G & Ref ₁ (%) | Hoover (%) |
| 95 | Normal | 71.38 | 73.83 | 72.42 | 83.85 |
| | Abnormal | 50.45 | 62.53 | 57.24 | 70.35 |
| | All images | 60.92 | 68.18 | 64.83 | 77.10 |
| 90 | Normal | 87.05 | 87.36 | 87.09 | 88.43 |
| | Abnormal | 76.46 | 81.64 | 78.40 | 81.08 |
| | All images | 81.75 | 84.50 | 82.74 | 84.76 |
| 85 | Normal | 91.08 | 91.03 | 91.37 | 90.62 |
| | Abnormal | 85.44 | 87.79 | 86.00 | 86.06 |
| | All images | 88.26 | 89.41 | 88.69 | 88.34 |
| 80 | Normal | 93.02 | 92.87 | 93.36 | 92.00 |
| | Abnormal | 89.67 | 90.81 | 89.94 | 88.96 |
| | All images | 91.35 | 91.84 | 91.65 | 90.48 |

Table 3

Effect of saturation condition

| Specificity (%) | Image type | Sensitivity | | | |
|-----------------|------------|-----------------------------|-----------|----------------------------|-----------|
| | | Before saturation condition | | After saturation condition | |
| | | Green (%) | R & G (%) | Green (%) | R & G (%) |
| 90 | Normal | 87.05 | 86.66 | 87.05 | 87.36 |
| | Abnormal | 76.46 | 79.83 | 76.46 | 81.64 |
| | All images | 81.75 | 83.41 | 81.75 | 84.50 |

Results show that the use of the proposed HM image instead of the green channel image improve the performance of the two-dimensional matched filter and offer better performance than using a reference model histogram and approximately the same performance as the Hoover method. At specificity of 90% in case of abnormal images, sensitivity increased from 76% when using the green channel image to 82% when using the HM image compared with 78% and 81% when using the reference histogram and the piece-wise threshold probing method, respectively. In case of normal images, at the same specificity, the sensitivity obtained when using green channel image, HM image, or reference histogram was 87% compared with 88% for the piece-wise threshold probing method. The performance of our method is evaluated by using a dataset of 20 images and a larger dataset is considered to be used in the future.

5. Conclusions

A new pre-processing method for retinal images is proposed. This method uses $\frac{2}{3}$ of the data (red and green channels) contained in colour digital fundus images instead of using $\frac{1}{3}$

of the available data (green channel only). In the process, we set a new criterion to test whether the test image is saturated or not. Applying the proposed method, a visual enhancement for retinal images in cases of non-uniform illumination is achieved and the performance of the two-dimensional matched filter is improved. This method can be used to pre-process retinal images before applying blood vessels segmentation methods as it results in decreasing the contrast between the abnormalities and the retinal background, and therefore can improve the performance of blood vessels segmentation methods.

Acknowledgements

The authors would like to thank A. Hoover for making the retinal images publicly available. N.M. Salem would like to acknowledge the financial support of the Egyptian Ministry of Higher Education, Egypt.

References

- [1] J. Evans, C. Rooney, F. Ashwood, N. Dattani, R. Wormald, Blindness and partial sight in England and Wales: April 1990–March 1991, *Health Trends* 28 (1996) 5–12.
- [2] F.L. Ferris, How effective are treatments for diabetic retinopathy?, *JAMA* 269 (1993) 1290–1291.
- [3] H.R. Taylor, J.E. Keefe, World blindness: a 21 century perspective, *Br. J. Ophthalmol.* 85 (3) (2001) 261–266.
- [4] T. Walter, J. Klein, P. Massin, A. Erginay, A contribution of image processing to the diagnosis of diabetic retinopathy detection of exudates in colour fundus images of the human retina, *IEEE Trans. Med. Imag.* 21 (10) (2002) 263–269.
- [5] D. Maberley, H. Walker, A. Koushik, A. Cruess, Screening for diabetic retinopathy in James Bay, Ontario: a cost-effectiveness analysis, *CMAJ* 168 (2) (2003) 160–164.
- [6] M. Shahidi, N.P. Blair, M. Mori, J. Gieser, J.S. Pulido, Retinal topography and thickness mapping in atrophic age related macular degeneration, *Br. J. Ophthalmol.* 86 (6) (2002) 623–626.
- [7] R.T. Smith, T. Nagasaki, J.R. Sparrow, I. Barbazetto, C. Klaver, J.K. Chan, A method of drusen measurement based on the geometry of fundus reflectance, *Biomed. Eng. Online* 2 (10) (2003).
- [8] A. Mora, J. Fonseca, P. Vieira, Drusen deposits modelling with illumination correction, *Proceedings of the IASTED International Conference on Biomedical Engineering*, 2005, pp. 80–85.
- [9] S. Chaudhuri, S. Chatterjee, N. Katz, M. Goldbaum, Detection of blood vessels in retinal images using two-dimensional matched filters, *IEEE Trans. Med. Imag.* 8 (3) (1989) 263–269.
- [10] T. Morris, Z. Newell, Enhancement and segmentation of retinal images, *Proceedings of the Time Frequency Time Scale '97*, University of Coventry, 1997.
- [11] C. Sinthanayothin, J.F. Boyce, H.L. Cook, T.H. Williamson, Automatic localisation of the optic disc, fovea, and retinal blood vessels from digital colour fundus images, *Br. J. Ophthalmol.* 83 (8) (1999) 902–910.
- [12] A. Osareh, M. Mirmehdi, B. Thomas, R. Markham, Automatic identification of diabetic retinal exudates in digital colour images, *Br. J. Ophthalmol.* 87 (10) (2003) 1220–1223.
- [13] K.A. Goatman, A.D. Whitwam, A. Manivannan, J.A. Olson, P.F. Sharp, Colour normalisation of retinal images, *Proceedings of the Medical Image Understanding and Analysis*, 2003, pp. 49–52.
- [14] M. Lalonde, L. Gagnon, M. Boucher, Automatic visual quality assessment in optical fundus images, *Proceedings of the Vision Interface '2001*, 2001, pp. 259–264.
- [15] L. Gagnon, M. Lalonde, M. Boucher, M.-C. Boucher, Procedure to detect anatomical structures in optical fundus images, *Proceedings of Conference Medical Imaging 2001: Image Processing (SPIE #4322)*, 2001, pp. 1218–1225.
- [16] C. Sinthanayothin, J.F. Boyce, T.H. Williamson, H.L. Cook, E. Mensah, S. Lal, D. Usher, Automatic detection of diabetic retinopathy on digital fundus images, *Diabetic Med.* 19 (2) (2002) 105–112.
- [17] F. Zana, J. Klein, A multimodal registration algorithm of eye fundus images using vessels detection and Hough transform, *IEEE Trans. Med. Imag.* 18 (5) (1999) 419–428.
- [18] A. Pinz, S. Bernogger, P. Datlinger, A. Kruger, Mapping the human retina, *IEEE Trans. Med. Imag.* 17 (4) (1998) 606–619.

- [19] A. Hoover, M. Goldbaum, Locating the optic nerve in a retinal image using fuzzy convergence of the blood vessels, *IEEE Trans. Med. Imag.* 22 (8) (2003) 951–958.
- [20] M. Foracchia, E. Grisan, A. Ruggeri, Detection of optic disc in retinal images by means of a geometrical model of vessel structure, *IEEE Trans. Med. Imag.* 23 (10) (2004) 1189–1195.
- [21] A. Hoover, V. Kouznetsova, M. Goldbaum, Locating blood vessels in retinal images by piece-wise threshold probing of a matched filter response, *IEEE Trans. Med. Imag.* 19 (3) (2000) 203–210.
- [22] L. Zhou, M.S. Rzeszutarski, L.J. Singerman, J.M. Chokreff, The detection and quantification of retinopathy using digital angiogram, *IEEE Trans. Med. Imag.* 13 (4) (1994) 619–626.
- [23] L. Gang, O. Chutatape, S.M. Krishnan, Detection and measurement of retinal vessels in fundus images using amplitude modified second-order Gaussian filter, *IEEE Trans. Biomed. Eng.* 49 (2) (2002) 168–172.
- [24] T. Chanwimaluang, G. Fan, An efficient algorithm for extraction of anatomical structures in retinal images, *Proc. IEEE Internat. Conf. Image Process.* (2003) 1093–1096.
- [25] X. Jiang, D. Mojon, Adaptive local thresholding by verification-based multithreshold probing with application to vessel detection in retinal images, *IEEE Trans. Pattern Anal. Mach. Intell.* 25 (1) (2003) 131–137.
- [26] J. Staal, M.D. Abramoff, M. Niemeijer, M.A. Viergever, B. van Ginneken, Ridge-based vessel segmentation in color images for the retina, *IEEE Trans. Med. Imag.* 23 (4) (2004) 501–509.
- [27] M. Niemeijer, J. Staal, B. van Ginneken, M. Long, M.D. Abramoff, Comparative study of retinal vessel segmentation methods on a new publicly available database, *Proc. SPIE Med. Imag.* 5370 (2004) 648–656.
- [28] R.C. Gonzalez, R.E. Woods, *Digital Image Processing*, Upper Saddle River, Prentice-Hall, NJ, 2002.
- [29] The STARE project: (<http://www.ces.clemson.edu/~ahoover/stare/>).
- [30] C.E. Metz, Basic principles of ROC analysis, *Semin. Nucl. Med.* 8 (4) (1978) 283–298.
- [31] T. Fawcett, ROC graphs: notes and practical considerations for researchers, HP Laboratories, Technical Report, 2004, HPL-2003-4.